2021

Testing the Efficacy of Surface Swab Sampling to Determine Post-Mortem Submersion Interval (PMSI), Using the Microbiome Colonization of Skeletal Remains Submerged in a Lotic Environment

Sarah Rose

2021

Testing the Efficacy of Surface Swab Sampling to Determine Post-Mortem Submersion Interval (PMSI), Using the Microbiome Colonization of Skeletal Remains Submerged in a Lotic Environment

Sarah Rose

Testing the Efficacy of Surface Swab Sampling to Determine Post-Mortem Submersion Interval (PMSI), Using the Microbiome Colonization of Skeletal Remains Submerged in a Lotic Environment

A thesis submitted in partial fulfillment of the requirements for the degree of Master of Science in Forensic Science at Virginia Commonwealth University

Sarah A. Rose

Date of Submission: 11 November 2021

Enrolled: Fall 2020, Spring 2021, & Fall 2021

Host Laboratory: Singh Laboratory
Department of Forensic Science - Virginia Commonwealth University

Research Mentor: Tal Simmons, PhD

ACKNOWLEDGEMENTS

Thank you to my support system, academic and otherwise, that made this work possible. I primarily must thank my advisor, research mentor, and friend, Dr. Tal Simmons. Your encouragement and support throughout my graduate studies has been a vital part of my success in the program. I would also like to extend thanks to the Singh lab, including Dr. Baneshwar Singh, for allowing me to join your lab and always encouraging me that positive outcomes were on the horizon, as well as Denise Wohlfahrt, whose technical guidance and support made my research possible. For my entire committee, including Dr. Tal Simmons, Dr. Baneshwar Singh, Dr. Jenise Swall, and Dr. Claire Cartozzo, I appreciate your support and patience in following me through this project during an incredibly challenging time. Many thanks to the faculty at Virginia Commonwealth University's Forensic Science Department for equipping me with the skills to become a better scientist and a proficient forensic scientist, as well as my classmates and colleagues who supported me along the way. Finally, I extend my deepest gratitude to my partner Greg; your unending patience and support, as well as your faith in my ability to change careers made all this possible, for which I will be forever grateful.

ABSTRACT

Estimating the post-mortem submersion interval (PMSI) can provide a valuable forensic tool for medicolegal death investigations involving victims discovered in aquatic environments. Previous studies conducted by Cartozzo et al. (2021) successfully demonstrated the use of microbial succession to create predictive models for the estimation of PMSI from submerged bone. Though effective, bone sampling requires time consuming processing techniques that result in destruction of decedent tissue. This study investigates the use of bone surface swabbing as an effective alternative method to bone sampling, with the goal of predicting PMSI using a simpler, non-invasive sampling technique. Porcine (*Sus scrofa*) skeletal remains (rib and scapulae) were caged and submerged in the James River at the Rice Rivers Center in Charles City, Virginia. One cage, containing five scapulae and five ribs, was collected every 250 ADD along with water samples (Cartozzo et al. 2021). In this study, swabs and water from the original experiment were analyzed at 500 ADD intervals, from baseline (0 ADD/0 days) to 4500 ADD (276 days). DNA was extracted from the swabs using the ChargeSwitch® gDNA Plant Kit and protocol, and variable region 4 (V4) of 16S rDNA was amplified and sequenced using the Illumina MiSeq Sequencing platform. Sequence analysis was performed with the Mothur (v.1.39.5) bioinformatics pipeline using the Mothur MiSeq SOP and R (v.4.1.1). Alpha diversity increased over the course of the study and Analysis of Molecular Variance (AMOVA) detected significant differences in beta diversity among bone, swab, and water groups ($p<0.001$, $F=6.32137$). These differences in beta diversity are likely explained by greater abundances of Clostridia and Gammaproteobacteria found in the bone samples compared to the swabs, and the overall variable presence and abundance of top taxa between bone and swab samples. Random forest models to predict PMSI were constructed using swabs for both ribs ($R^2=0.822$ and RMSE=600.6 ADD vs. $R^2=0.94$, RMSE=477 ADD in bone) as well as scapulae ($R^2=0.766$ and RMSE=681.4 ADD vs. $R^2=0.93$, RMSE=501 ADD in bone). Swab samples predicted PMSI, albeit less accurately than bone powder, though this may well be due to the reduced sample of swabs (n=34) used in this study compared to bone (n=54). These results suggest that further investigation into bone surface swabbing is warranted, as improved models may provide an accurate, less labor-intensive, and non-destructive alternative for sampling skeletal remains to perform microbial PMSI prediction.

INTRODUCTION

Determining the postmortem interval (PMI) can provide crucial information and investigative leads for medicolegal death investigators. Forensic investigations may require PMI estimates to aide in victim identification and determining the circumstances of death, as well as to corroborate witness and suspect accounts in homicide casework. In water-related body discoveries, such as accidental drownings or clandestine victim disposals, sinking of the body initially or later in decomposition may increase the time required to recover the remains. Extended PMI can cause degradation and loss of physical forensic evidence, and potentially a more advanced decomposition state upon discovery. Of particular relevance for skeletal remains, quantitative methods of assessing decomposition state in the absence of soft tissue are necessary to produce a more accurate, useful PMI for investigators.

The postmortem submersion interval (PMSI) describes the time elapsed between entry into the water and recovery of a decedent. Estimating PMSI through current quantitative methods involves relating the physical decomposition state of a decedent to time and preferably temperature. The Aquatic Decomposition Scoring (ADS) technique utilizes a points-based scoring system of the body's physical appearance as it relates to decomposition, the sum of which (Total Aquatic Decomposition Score, or TADS) can accurately (R^2=0.71) predict PMSI [1]. Accumulated degree days (ADD), which utilizes the cumulative summation of daily temperatures to quantify temperature temporally, has also been used to refine prediction of PMSI from ADS, as temperature and time strongly influence decomposition rates [2]. PMSI approaches also use ADD, but substitute ambient water temperature for air temperature to more accurately account for time and temperature in an aquatic environment [3].

Along with time and temperature, colonization of necrophagous insects on cadavers also influences decomposition [4], [5]. Though useful in terrestrial PMI models, necrophagous insects do not have continuous access to remains in aquatic environments (due to changes in buoyancy and submersion) which prevents the use of entomological colonization and succession for estimating PMSI. Submerged remains may instead host various organisms that have been used to estimate PMSI, including barnacles [6], fungi [7], algae [8], and diatoms [9]. However, regardless of submersion state, bacteria provide a similar ecological influence in decomposition for PMSI that may be considered analogous to the insect model. Specifically, bacteria drive decomposition starting in the early stages of decomposition.

Decomposition begins with autolysis, which initiates the breakdown of body tissues at a cellular using compounds endogenous to the body (i.e., lysozymes). Putrefaction initiates with the cessation of autolysis, driven by microbes that colonized the body in life. Endogenous anaerobic bacteria found in the enteric and respiratory systems typically begin proliferating and invade surrounding tissues. Though anaerobic bacteria dominate the postmortem fauna, facultative anaerobic and aerobic bacteria colonize the remains as decomposition continues. As such, the microbial community of remains provide a rich, diverse community that may be exploited to better understand the stages of decomposition and estimate PMSI in a quantitative manner. [10]

Overall, research exploring quantitative measures for PMSI remains relatively sparse in the literature compared to PMI. The first studies to used microbial colonization of human remains to apply bacterial succession techniques to PMSI estimation using cloning techniques to perform bacterial colonization and subsequent analysis [11]. These techniques used succession and changes of relative abundance in microbial communities, as well as the presence of indicator taxa to create models for PMSI prediction. Advancements in Next Generation Sequencing (NGS) have further

improved capabilities and access to molecular techniques in forensics, especially for microbiome-based work by using DNA sequencing to target specific genomic regions to identify taxa in massively parallel analyses [12], [13].

The literature contains often short-term studies of PMSI with far fewer studies overall compared to PMI, often studied over a time course of less than a month [14]–[18], with even fewer using long-term studies of PMSI. Studies using microbiome succession to predict long-term PMSI have used direct sampling of porcine skeletal remains in both lentic and lotic aquatic habitats [19], [20], as well as surface swabbing sampling of a fully-fleshed porcine carcass in a two-season lotic environment [21]. Studies by Cartozzo et al. [19], [20] using powdered bone demonstrated the use of microbial succession and produced an accurate PMSI model across a lengthy time series.

Though effective, bone sample processing is a destructive and time-consuming technique that typically requires specialized equipment and personnel to cut and process bones into a powder fine enough to enable sufficient DNA extraction from often degraded samples. Compared to swab samples, which are utilized frequently for reference DNA profiles and collecting evidence, bone samples are less commonly processed in forensic biology laboratories. Skin microbiome studies primarily use swabs to sample the microbial community in human medical studies [22], [23] and in human cadavers [24], [25]. The use of skeletal swabs to obtain a representative microbial community is not noted in the literature, but represents a forensically relevant time series, as PMSI models could be most applicable to partial remains or remains devoid of tissue. Since surface swabbing provides a simple, non-destructive technique requiring no costly processing equipment, conserves sample, and minimizes processing time, its use for sampling the microbial community on skeletal remains for estimating PMSI should be explored.

This study aims to determine whether surface swabs of skeletal remains in a lotic, freshwater river environment provide an effective technique for estimating PMSI, using targeted metagenomic sequencing of the 16S rDNA region of bacteria. Bone surface swabs collected from porcine skeletal remains submerged in a lotic environment will be used to evaluate differences in bacterial community structure between swab and bone sample types as well as to create a model for predicting PMSI. Comparison of the predictive models for PMSI in bone surface swabs and bone powder will be used to evaluate the utility of using swabs as an alternative to bone sampling.

METHODS

Sample Collection

Sample collection was performed as outlined in Cartozzo et al. 2021 [19]. Briefly, 24 10" x 10" cages containing porcine (*Sus scrofa*) ribs and scapulae were submerged in the James River at the Rice Rivers Center in Charles City, Virginia, USA (37.3260 °N, 77.2056 °W). Five scapulae and five ribs were frozen without prior submersion as baseline/0 ADD samples. Starting at 250 ADD, one cage containing five scapulae and five ribs was pulled for sampling and frozen at -80 °C every 250 ADD until all cages were removed from the river. Bone surface swabs were collected within six months of bone collection, once bones were thawed and cleaned (i.e., removal of adipocere) using sterile cotton tipped swabs and frozen at -20 °C until analysis. Additionally, water samples were collected at each time series and filtered using a 0.22 μm filter and stored at 4 °C until analysis. This study targeted three surface swabs from ribs and scapulae in 500 ADD intervals, from 0 ADD to 4500 ADD, as well as one water sample per collection (Table 1). Due to physical sample loss during submersion (n=2), 28 rib and 30 scapula swab and bone samples were used for downstream DNA analysis.

DNA Extraction:

DNA was extracted from the bone surface swabs using the ChargeSwitch® gDNA Plant Kit (Life Technologies, Grand Island, NY), following the Invitrogen CST Protocol for Extracting gDNA from Bone Samples, with 100 µl used as the final elution volume [26]. DNA extracts were quantified using the Invitrogen™ Qubit® 2.0 Fluorometer directly following extraction and the remaining extract was stored at -20 °C until further analysis.

16S rDNA Amplification and MiSeq® Sequencing-by-Synthesis:

Variable region four (V4) of the 16S rRNA gene (16S rDNA) was amplified using the Kozich et al. dual-index primer technique [27], using the Veriti™ 96-Well Thermal Cycler (Applied Biosystems, USA) to perform polymerase chain reaction (PCR). ZymoBIOMICS™ DNA extract was used as the mock community standard and ddH_20 was used as the negative control. Reactions were performed in 20 µL, including the following components: template DNA (up to10 ng in 6.2 µL maximum volume), 10 µL Promega PCR master mix (2X), 0.8 µL 25 nM $MgCl_2$ and 3 µL of forward/reverse primers (10 µM each):

V4_515F 5'- AATGATACGGCGACCACCGAGATCTACACXXXXXXXXTATGGTAATTGTGTGYCAGCMGCC GCGGTAA-3'

806R:5'- CAAGCAGAAGACGGCATACGAGATXXXXXXXXAGTCAGTCAGCCGGACTACNVGGGTWTC TAAT-3'.

Agarose gel electrophoresis (AGE; 1.5-2.0%) was used to confirm the presence of high-molecular weight amplicons and PCR success using 2 µL of 6X loading dye (New England Biolabs, MA, USA), 7 µL of 1X TAE buffer, and 3 µL of PCR product.

For samples that failed to amplify, tenfold dilutions were performed using ddH_20 as the diluent before repeating PCR and AGE. If samples failed to amplify after dilution, a modified QIAGEN® DNeasy® PowerClean Cleanup Kit cleaning procedure was used, using isopropanol instead of ethanol [28].

Post-PCR cleanup was performed using Agencourt® AMPure® PCR Purification kit (Beckman Coulter, Brea, CA), according to the manufacturer's protocol, was be used to purify 10 μL of the remaining 17 μL PCR product [29]. The Invitrogen™ Qubit 2.0 Fluorometer was used to quantify each sample following purification. Samples were then diluted to 1 ng/μL and pooled before using the Savant DNA120 Speed Vac Concentrator (Fisher Scientific, Waltham, MA) to concentrate pooled samples to 1 ng/μL. Sequencing (2x250 paired-end sequencing-by-synthesis) was performed using the Illumina MiSeq® v2 Reagent Kit and Illumina MiSeq® FGx system (Illumina, San Diego, CA).

Sequence Analysis:

Mothur software (v. 1.39.5) and the mothur MiSeq SOP (https://mothur.org/wiki/miseq_sop/) was used to process raw sequencing data [30], [31]. Forward and reverse reads were assembled into contigs (*make.contig* command), and then quality control measures were performed to remove ambiguous bases, reads greater than 275 bp and less than 200 bp, and duplicate sequences. Next, unique sequences of appropriate length were aligned to the SILVA bacterial reference [32]. Once alignment was complete, sequences that failed to align properly or started or ended beyond the target region (13862-23444) were removed. Chimeric sequences were also removed using UCHIME [33]. The data was sorted taxonomically using Naïve Bayesian rRNA classifier v. 2.2 [34] based on the Greengenes 13_8_99 reference database [35], using a bootstrapping cutoff of >80%. After classification, non-bacterial sequencies (i.e., mitochondria, chloroplasts, eukaryote, archaea, unknown) were removed. Sequences from this step were used for data analysis using relative abundance, including class-level taxonomy for sample groups, indicator taxa analysis, and creating random forest models.

Rarefaction curves using Operational Taxonomy Units (OTUs) by sequencing cycle at 3%, 5%, and 10% genetic distance were evaluated to gauge the appropriate genetic distance and subsequent subsampling level (Figure 1). Random subsampling to normalize taxonomy data was performed at a cutoff of 4,900 reads per sample using a genetic distance of 5% at the hypothetical genus level, resulting in the loss of six swab samples and the negative controls. Once subsampled, coverage for OTUs for each sample group was 96.5% and 96.7% for rib and scapula swabs, respectively, 97.3% and 95.0% for rib and scapula bone samples, respectively, and 93.1% for water. Subsampled taxonomic data were then used to calculate phylogenetic distances and perform statistical tests detailed in "Data Analysis."

Data Analysis:

Microsoft Excel (2016) software was used to further organize and visualize taxonomic data, including relative and abundance graphs at the class level, and to process data for analysis in statistical softwares.

In addition to sequence analysis, alpha diversity was calculated using mothur using the *summary.single* command at 5% genetic distance using the Simpson, Inverse Simpson and Shannon indices, along with percent coverage. Non-metric multidimensional scaling (NMDS) ordination plot axes were calculated using the *nmds* command.

The statistical software R (4.1.1) [36], and associated packages were used to analyze indicator taxa (using the indicspecies package [37]) and to create NMDS ordination plots (using the rgl pckage [38]) to visualize group differences in sample type, bone type, and ADD. The predicted PMSI was calculated using random forest modeling using relative abundance of

taxonomy at the family level, using the randomForest package and modeling method outlined by Forger et al. 2019 [39].

RESULTS

Sequence Characteristics:

A total of 104 samples, including bone (n=54), swab (n=34), water (n=10), mock positive (n=1), and negative controls (n=5), produced 2,229,017 sequence reads, including 1,399,870 from bone samples, 572,693 from swabs, and 172,385 from water (Table 2). Fifty-eight percent of initial sequence reads were lost during quality control steps. Remaining final reads used for further data analysis included 1,291,253 reads, with 840,027 reads for bone (15,556 average reads per sample), 362,745 for swabs (10,669 average reads per sample), and 75,515 for water (7,552 average reads per sample) (Table 3).

Taxonomy Analysis

For the bone, swab, and water samples, a total of 1,312,651 sequences were classified into 70 phyla, 165 classes, 241 orders, 281 families, 561 genera, and 331 species. Relative abundance was calculated for each sample type at the class level and visualized using the top 15 taxa, with the remaining taxa categorized into unclassified and rare taxa (Figure 2, Figure 3).

Yue & Clayton (thetayc) distance matrices were used for AMOVA (Analysis of Molecular Variance) and visualization of data in NMDS plots. AMOVA of the bacterial structure associated with swab, bone, and water samples indicated significant differences amongst sample groups ($p<0.001$, $F = 6.32137$) (Table 4). Visualized using a 3D NMDS plot, the sample groups are generally clustered, with water exhibiting the best overall inter-group resolution (Figure 4). In

terms of overall relative abundance trends, the rib and scapula bone samples and the rib and scapula swab samples each shared more taxa in common within their sample type group than between sample types, and water was comprised of overall different taxa than both bone and swab sample types (Figure 2, Figure 3). AMOVA of the bacterial structure associated with bone and swab samples by bone type indicated significant differences between rib and swab bones ($p=0.002$, $F=2.96807$), but not between rib and scapula swab samples ($p=0.247$, $F=1.1935$) (Table 5). A 3D NMDS ordination plot of rib and scapula swab samples was used to visualize the two groups and shows overlap between the swab types with no clear grouping ($R^2=0.726$; lowest stress=0.191) (Figure 5). When both bone swab types were combined and the effect of ADD was tested, AMOVA again indicated differences between ADD ($p<0.001$, $F=3.67184$), with the most significant differences detected across larger ADD differences (Table 6). A 3D NMDS ordination plot of ADD for combined swab samples showed some clear clustering, most notably with the baseline (0 ADD) samples ($R^2=0.726$; lowest stress=0.191) (Figure 6).

Though Clostridia was found in all four samples, this taxon was more abundant in the bone samples than in both swab types, and Clostrida decreased over time in each sample group. Bone samples also shared Holophagae (not found in swabs) and Bacteriodia (found in scapula swabs) taxa in common. Swab samples also shared Alphaproteobacteria and Betaproteobacteria in common, neither of which taxa were found in the bone sample but were found in the water samples. The water samples were primarily composed of Synechococcophycideae and Actinobacteria.

For the bone and swab samples, the community composition changed markedly from 0 ADD (baseline, unsubmerged) to 500 ADD. For these four groups, Gammaproteobacteria was the predominant taxon found across the groups at 0 ADD and the relative abundance of Gammaproteobacteria dropped precipitously starting at 500 ADD. At 500 ADD, Clostridia was

found in high, but decreasing relative abundance in the bone samples throughout the time series and was most abundant in the swab samples between 500 and 1000 ADD. Composition in the water samples remained fairly stable across ADD, with Synechococcophycideae peaking in abundance at 3000 ADD. (Note: data from 500-2500 ADD were excluded from the water dataset during sequence processing, limiting trend interpretation.)

Indicator taxa were evaluated using the 50 most abundant genera. Water exhibited the highest point biserial correlation coefficient (PBCC) values (Table 7). PBBC values for water were the only values greater than 0.5 with a p-value <0.001. Unclassified ACK.M1 and R4.41B from the water group had PBCC values >0.9, with the remaining top 10 indicator genera representing either water, or a combination of groups as indicators. Individually for the bone and swab samples, several taxa were identified as indicators, albeit with a low PBCC (<0.5), weakening the significance of these taxa as indicators (Table 8, Table 9). Similarly, a heat map visualizing indicators in bone, swab, and water samples visualizes this overall lack of clear indicator genera found and similarity in structure among bone samples as well as swab samples, with the exception of the taxa noted in the water samples (Table 7), and in the bone samples (Clostridium and unclassified Veillonellaceae and Clostridales) (Figure 7).

Overall, phylogenetic alpha diversity fluctuated but increased with ADD, with the most notable increase occurring between 0 and 1000 ADD (Figure 8). Scapula and rib swab samples reached their peak level of phylogenetic diversity at 3000 and 3500 ADD, respectively, and scapula and rib bone samples similarly reached peak phylogenetic diversity at 3000 and 4000 ADD, respectively. Alpha diversity was also assessed using Inverse Simpson, Shannon, and Shannon Evenness Indices, which similarly showed fluctuations in alpha diversity along the time series (Table 10). Due to sample loss at various time points in the swab samples, limited data exists to

draw further conclusions for broad trends in phylogenetic alpha diversity and the diversity indices used.

PMSI Predictive Model

Using taxonomy abundance data prior to subsampling, random forest modeling was used to construct predictive PMSI models for rib and scapula swabs, both with and without baseline (0 ADD) observations. Excluding the baseline observations, using 15 rib swab observations and 49 family-level taxa, rib swabs produced a model with R^2=0.731 and a root mean square error (RMSE) of 642.7 ADD, or approximately 39.4 days (Figure 9). Influential taxa included (in order of greatest decrease in RMSE to least) Bacteroidaceae, Veillonellaceae, Pirellulaceae, Enterobacteriaceae, and Synechococcaceae (Figure 10). With baseline observations included, 18 rib swab observations and 49 family-level taxa were used to produce a model with R^2=0.822 and RMSE=600.6 ADD, or approximately 36.8 days (Figure 11). Influential taxa included Methylococcaceae, Holophagaceae, Rhodospirillaceae, Xanthromonadaceae, and Pirellulaceae (Figure 12).

Using 14 scapula swab observations and 53 family-level taxa, scapula swabs produced a model with R^2=0.566 and RMSE=800.9 ADD, or approximately 49.1 days (Figure 9). Influential taxa included (in order of greatest decrease in RMSE to least) Clostridiaceae, Methylococcaceae, Methylocystaceae, Moraxellaceae, Crenotrichaceae, and Enterobacteriaceae (Figure 10). With baseline observations included, 17 observations and 49 family-level taxa were used to produce a model with R^2=0.766 and RMSE=681.4 ADD, or approximately 41.8 days (Figure 11). Influential taxa included Methylococcaceae, Methylocystaceae, Moraxellaceae, Crenotrichaceae, Pseudomonadaceae, Pirellulaceae, and Holophagaceae (Figure 12).

DISCUSSION

This study assessed whether bone surface swabbing could provide a sampling of the bacterial community from remains that was representative of the remains or otherwise yielded bacterial succession data that may be used to create predicted PMSI models. Using 16S rDNA sequencing, trends in bacterial succession and overall diversity were observed across ADD, but the community on the surface of the bone, collected using swabs, produced different community characteristics than bone. Though slight differences in bacterial community between bone types (rib and scapula) were found in previous studies, AMOVA statistical tests found differences between bone, swab, and water samples, and no significant difference between rib swabs and scapula swabs.

Differences in taxa were notable at the class level both in the taxa present, relative abundance of those taxa, and the fluctuations in relative abundance across ADD. Importantly, baseline data for the bone and swab samples exhibited notably different taxonomy than the subsequent ADD samples, as would be expected from fresh remains experiencing little to no decay and not exposed to an experimental treatment. Clostridia comprised the highest overall relative abundance in the bone samples starting at 500 ADD and remained an abundant taxon throughout the time series, though the relative abundance of Clostridia decreased over time. The swab sample bacterial community contained relatively abundant Clostridia early in the time series, between 500 and 1000-1500 ADD, before dropping precipitously and remaining in low relative abundance for the rest of the time series. Once Clostridia decreased in the swab samples, additional taxa including Alphaproteobacteria, Betaproteobacteria, and Deltaproteobacteria rose in relative abundance.

These taxa were also present in the bone samples, but in lower relative abundance as Clostridia maintained relatively high abundance. Gammaproteobacteria was also noted in high relative abundance in the 0 ADD samples for all sample groups and steadily decreased over the time series, with the most notable decrease occurring between 0 and 500 ADD.

Taxa belonging to Clostridia (genus Clostridium and unclassified taxa from families Veillonellaceae and Clostridales) were also among the most notable in genus relative abundance heat map (Figure 7) in the bone samples throughout much of the time series, with Clostridium also represented in earlier ADD in the swab samples. Unlike the influential taxa found in the water samples which occurred consistently throughout the time series in the heat map, the influential taxa in the bone and swab samples fluctuated in abundance, likely diminishing their overall influence as calculated by indicator analysis performed in R (indicspecies).

Linked to the formation of adipocere, the presence of Clostridia during decomposition is well reported in the literature in both terrestrial [40]–[42] and aquatic studies [18]–[21] and the presence of this taxon likely represents endogenous bacteria from the porcine remains partially driving decomposition. The differences in abundance of Clostridia between the bone and swab samples, with higher relative abundance of this taxon in bone samples, likely represent the disparate presence of endogenous and exogenous bacteria as drivers of decomposition in the two sample types. In the bone samples, a greater proportion of endogenous bacteria likely drives decomposition from within the bone with exogenous bacteria contributing to a lesser extent. In the swab samples, after ~1000 ADD, exogenous bacteria appear to primarily drive decomposition on the surface of the bone, as detected by the swabs.

Notably, the overall taxonomic structure of the water samples appeared different and less diverse than both the bone and swab samples. Taxa found in the water were common to the bone

and swab samples, though no striking similarities with respect to relative abundance exist among the groups and water. For submerged remains, water would be expected to provide a potential source of microbes colonizing remains, though the taxonomic results of this study suggest otherwise. Instead of water as a source of exogenous drivers of decomposition, particularly in a continually flowing, lotic environment, the benthic substrate may provide a more robust and stable microbial community that influences the community structure to a greater degree.

For both bone and swab sample types, a general increase in alpha diversity was observed, similar to the results reported by Cartozzo et al. [19], [20]. Beta diversity, tested by AMOVA among sample types (bone, swab, water), and all types (rib bone, scapula bone, rib swab, scapula swab, and water) supported broad group differences among sample types observed in the taxonomic data, and no significant differences indicated between swab rib and swab scapula groups. Beta diversity across ADD was dissimilar and less distinct in the swab samples compared to the ADD resolution found in the Cartozzo et al. [19] bone samples for the same environment, though the most distinct groups, such as the baseline ADD compared to subsequent ADD, can be resolved fairly well. Again, the low number of samples for some time points may reduce the ability of the NMDS analysis approach to differentiate between the ADD groupings.

Overall, PMSI models constructed with swab data performed less accurately than those constructed with bone data in Cartozzo et al.'s [18] freshwater river study. Both models explained less variance in the samples as evidenced by R^2 values for ribs and scapulae (up to 82.2% and 76.6%, respectively versus 94% in bone), as well as greater RMSE (600.6 and 681.4 ADD, respectively, versus 477 and 501 ADD in bone). The bacterial community found on scapula swabs predicted PMSI less accurately than rib swabs, similar to Cartozzo et al., where scapula bones predicted PMSI less accurately than rib bones [18]. Also similar to the bone PMSI models, the

underlying influential taxa did not need to be in high relative abundance to inform the model. Though different taxa influenced succession in the bone and swab samples and may contribute to the lowered ability of the random forest models to predict PMSI, sample loss resulting in fewer data for comparison likely contributes considerably to the issues of model accuracy.

CONCLUSION

This study found that bone surface swabs of the microbial community found on submerged skeletal porcine bones produced a model for predicting PMSI, though with less accuracy than bone powder. The main factors that affected the accuracy of the PMSI model include both the notably different taxa and trends in taxa across ADD along with limited indicator taxa found in the bone surface swabs, as well as the reduced number of samples used for the model due to sample loss and inhibition. Overall, significant differences were noted between the bone powder and bone swabs, with no significant differences between rib and scapula swabs. Broadly, bacterial succession found in bone powder likely represents the temporal decrease of endogenous taxa as exogenous taxa increases, whereas swab samples likely represent primarily exogenous taxa. Notably, as the taxa found in the water samples were distinct from taxa found in the bone surface swabs, this suggests that exogenous taxa originate from another source, such as benthic substrate or other invertebrate that might have colonized submerged bones.

Future studies should continue to target long-term time series to capture forensically relevant post-mortem intervals. For post-mortem submersion interval, various aquatic environments should also be targeted to explore the effect of water system type and substrate on remains and surface swabs of remains. Additionally, fully fleshed porcine remains should be tested in a similarly lengthy time series, and eventually translated to human cadaver studies. Due to the

similar testing workflow, similar targeted metagenomic approaches using 18S rDNA and ITS regions should also be explored in tandem with 16S rDNA to evaluate the relative effectiveness of each target community, and whether this effectiveness is dependent upon cadaver deposition environment.

REFERENCES

[1] M. A. van Daalen *et al.*, "An Aquatic Decomposition Scoring Method to Potentially Predict the Postmortem Submersion Interval of Bodies Recovered from the North Sea," *J. Forensic Sci.*, vol. 62, no. 2, pp. 369–373, 2017, doi: 10.1111/1556-4029.13258.

[2] C. Palazzo *et al.*, "Application of aquatic decomposition scores for the determination of the Post Mortem Submersion Interval on human bodies recovered from the Northern Adriatic Sea," *Forensic Sci. Int.*, vol. 318, p. 110599, 2021, doi: 10.1016/j.forsciint.2020.110599.

[3] V. Heaton, A. Lagden, C. Moffatt, and T. Simmons, "Predicting the postmortem submersion interval for human remains recovered from U.K. waterways," *J. Forensic Sci.*, vol. 55, no. 2, pp. 302–307, 2010, doi: 10.1111/j.1556-4029.2009.01291.x.

[4] T. Simmons, R. E. Adlam, and C. Moffatt, "Debugging decomposition data - Comparative taphonomic studies and the influence of insects and carcass size on decomposition rate," *J. Forensic Sci.*, vol. 55, no. 1, pp. 8–13, 2010, doi: 10.1111/j.1556-4029.2009.01206.x.

[5] J. Dalal, S. Sharma, T. Bhardwaj, S. K. Dhattarwal, and K. Verma, "Seasonal study of the decomposition pattern and insects on a submerged pig cadaver," *J. Forensic Leg. Med.*, vol. 74, no. January, p. 102023, 2020, doi: 10.1016/j.jflm.2020.102023.

[6] P. A. Magni, E. Tingey, N. J. Armstrong, and J. Verduin, "Evaluation of barnacle (Crustacea: Cirripedia) colonisation on different fabrics to support the estimation of the time spent in water by human remains," *Forensic Sci. Int.*, vol. 318, p. 110526, Jan. 2021, doi: 10.1016/J.FORSCIINT.2020.110526.

[7] C. Hyun, H. Kim, S. Ryu, and W. Kim, "Preliminary study on microeukaryotic community analysis using NGS technology to determine postmortem submersion interval (PMSI) in the drowned pig §," *J. Microbiol.*, vol. 57, no. 11, pp. 1003–1011, 2019, doi: 10.1007/s12275-019-9198-0.

[8] J. N. Haefner, J. R. Wallace, and R. W. Merritt, "Pig Decomposition in Lotic Aquatic Systems: The Potential Use of Algal Growth in Establishing a Postmortem Submersion Interval (PMSI)," *J. Forensic Sci.*, vol. 49, no. 2, pp. 1–7, 2004, doi: 10.1520/jfs2003283.

[9] K. A. Zimmerman and J. R. Wallace, "The potential to determine a postmortem submersion interval based on algal/diatom diversity on decomposing mammalian carcasses in brackish ponds in Delaware," *J. Forensic Sci.*, vol. 53, no. 4, pp. 935–941, 2008, doi: 10.1111/j.1556-4029.2008.00748.x.

[10] Ralebitso-Senior, T. Komang, *Forensic Ecogenomics: The Application of Microbial Ecology Analyses in Forensic Contexts*. Academic Press, 2018.

[11] G. C. Dickson, R. T. M. Poulter, E. W. Maas, P. K. Probert, and J. A. Kieser, "Marine bacterial succession as a potential indicator of postmortem submersion interval," *Forensic Sci. Int.*, vol. 209, no. 1–3, pp. 1–10, 2011, doi: 10.1016/j.forsciint.2010.10.016.

[12] E. R. Hyde, D. P. Haarmann, J. F. Petrosino, A. M. Lynne, and S. R. Bucheli, "Initial insights into bacterial succession during human decomposition," *Int. J. Legal Med.*, vol. 129, no. 3, pp. 661–671, 2015, doi: 10.1007/s00414-014-1128-4.

[13] J. L. Pechal, T. L. Crippen, M. E. Benbow, A. M. Tarone, S. Dowd, and J. K. Tomberlin, "The potential use of bacterial community succession in forensics as described by high throughput metagenomic sequencing," *Int. J. Legal Med.*, vol. 128, no. 1, pp. 193–205, 2014, doi: 10.1007/s00414-013-0872-1.

[14] J. R. Wallace, J. P. Receveur, P. H. Hutchinson, S. F. Kaszubinski, H. E. Wallace, and M.

E. Benbow, “Microbial community succession on submerged vertebrate carcasses in a tidal river habitat: Implications for aquatic forensic investigations,” *J. Forensic Sci.*, vol. 66, no. 6, pp. 2307–2318, 2021, doi: 10.1111/1556-4029.14869.

[15] J. L. Pechal and M. E. Benbow, “Microbial ecology of the salmon necrobiome: Evidence salmon carrion decomposition influences aquatic and terrestrial insect microbiomes,” *Environ. Microbiol.*, vol. 18, no. 5, pp. 1511–1522, 2016, doi: 10.1111/1462-2920.13187.

[16] K. Fujii, S. Inokuchi, T. Kitayama, H. Nakahara, N. Mizuno, and K. Sekiguchi, “A comparison of DNA extraction using automate express™ and EZ1 advanced XL from liquid blood, bloodstains, and semen stains,” *J. Forensic Sci.*, vol. 58, no. 4, pp. 981–988, 2013, doi: 10.1111/1556-4029.12174.

[17] R. Zhou, Y. Wang, M. G. Hilal, Q. Yu, T. Feng, and H. Li, “Temporal succession of water microbiomes and resistomes during carcass decomposition in a fish model,” *J. Hazard. Mater.*, vol. 403, no. July 2020, p. 123795, 2021, doi: 10.1016/j.jhazmat.2020.123795.

[18] J. He, J. Guo, X. Fu, and J. Cai, “Potential use of high-throughput sequencing of bacterial communities for postmortem submersion interval estimation,” *Brazilian J. Microbiol.*, vol. 50, no. 4, pp. 999–1010, 2019, doi: 10.1007/s42770-019-00119-w.

[19] C. Cartozzo, T. Simmons, J. Swall, and B. Singh, “Postmortem submersion interval (PMSI) estimation from the microbiome of Sus scrofa bone in a freshwater river,” *Forensic Sci. Int.*, vol. 318, p. 110480, 2021, doi: 10.1016/j.forsciint.2020.110480.

[20] C. Cartozzo, B. Singh, J. Swall, and T. Simmons, “Postmortem submersion interval (PMSI) estimation from the microbiome of sus scrofa bone in a freshwater lake,” *J. Forensic Sci.*, vol. 66, no. 4, pp. 1334–1347, 2021, doi: 10.1111/1556-4029.14692.

[21] M. E. Benbow, J. L. Pechal, J. M. Lang, R. Erb, and J. R. Wallace, “The Potential of High-throughput Metagenomic Sequencing of Aquatic Bacterial Communities to Estimate the Postmortem Submersion Interval,” *J. Forensic Sci.*, vol. 60, no. 6, pp. 1500–1510, 2015, doi: 10.1111/1556-4029.12859.

[22] S. Prast-Nielsen *et al.*, “Investigation of the skin microbiome: swabs vs. biopsies,” *Br. J. Dermatol.*, vol. 181, no. 3, pp. 572–579, 2019, doi: 10.1111/bjd.17691.

[23] J. S. Meisel *et al.*, “Skin Microbiome Surveys Are Strongly Influenced by Experimental Design,” *J. Invest. Dermatol.*, vol. 136, no. 5, pp. 947–956, 2016, doi: 10.1016/j.jid.2016.01.016.

[24] G. T. Javan, S. J. Finley, Z. Abidin, and J. G. Mulle, “The thanatomicrobiome: A Missing Piece of the Microbial Puzzle of Death,” *Front. Microbiol.*, vol. 7, no. FEB, 2016, doi: 10.3389/fmicb.2016.00225.

[25] S. Pittner *et al.*, “The applicability of forensic time since death estimation methods for buried bodies in advanced decomposition stages,” *PLoS One*, vol. 15, no. 12 December, pp. 1–26, 2020, doi: 10.1371/journal.pone.0243395.

[26] Invitrogen, “CST Protocol for Extracting gDNA from Bone Samples,” 2009. https://assets.thermofisher.com/TFS-Assets/LSG/manuals/gDNAbone_short_protocol.pdf (accessed Sep. 09, 2020).

[27] J. J. Kozich, S. L. Westcott, N. T. Baxter, S. K. Highlander, and P. D. Schloss, “Development of a dual-index sequencing strategy and curation pipeline for analyzing amplicon sequence data on the miseq illumina sequencing platform,” *Appl. Environ. Microbiol.*, vol. 79, no. 17, pp. 5112–5120, 2013, doi: 10.1128/AEM.01043-13.

[28] Qiagen, “DNeasy® PowerClean Cleanup Kit: Quick-Start Protocol,” 2016. .

[29] Agencourt, “AMPure PCR Purification Instructions for Use,” 2013.

https://www.beckmancoulter.com/wsrportal/techdocs?docname=B37419AA (accessed Nov. 11, 2020).
[30] P. D. Schloss *et al.*, "Introducing mothur: Open-source, platform-independent, community-supported software for describing and comparing microbial communities," *Appl. Environ. Microbiol.*, vol. 75, no. 23, pp. 7537–7541, 2009, doi: 10.1128/AEM.01541-09.
[31] P. D. Schloss, "Reintroducing mothur: 10 Years Later," *Appl. Environ. Microbiol.*, vol. 86, no. 2, p. 13, 2020.
[32] C. Quast *et al.*, "The SILVA ribosomal RNA gene database project: Improved data processing and web-based tools," *Nucleic Acids Res.*, vol. 41, no. D1, pp. 590–596, 2013, doi: 10.1093/nar/gks1219.
[33] R. C. Edgar, B. J. Haas, J. C. Clemente, C. Quince, and R. Knight, "UCHIME improves sensitivity and speed of chimera detection," *Bioinformatics*, vol. 27, no. 16, pp. 2194–2200, 2011, doi: 10.1093/bioinformatics/btr381.
[34] Y. Karaca and C. Cattani, "7. Naive Bayesian classifier," *Comput. Methods Data Anal.*, pp. 229–250, 2018, doi: 10.1515/9783110496369-007.
[35] T. Z. DeSantis *et al.*, "Greengenes, a chimera-checked 16S rRNA gene database and workbench compatible with ARB," *Appl. Environ. Microbiol.*, vol. 72, no. 7, pp. 5069–5072, 2006, doi: 10.1128/AEM.03006-05.
[36] D. C. Dirkmaat and L. L. Cabo, "Forensic Archaeology and Forensic Taphonomy: Basic Considerations on how to Properly Process and Interpret the Outdoor Forensic Scene," *Acad. Forensic Pathol.*, vol. 6, no. 3, pp. 439–454, 2016, doi: 10.23907/2016.045.
[37] M. De Caceres, "How to use the indicspecies package (ver.1.7.1)," \, p. 29, 2013.
[38] O. Nenadić and M. Greenacre, "Correspondence analysis in R, with two- and three-dimensional graphics: The ca package," *J. Stat. Softw.*, vol. 20, no. 3, pp. 1–13, 2007, doi: 10.18637/jss.v020.i03.
[39] L. V. Forger, M. S. Woolf, T. L. Simmons, J. L. Swall, and B. Singh, "A eukaryotic community succession based method for postmortem interval (PMI) estimation of decomposing porcine remains," *Forensic Sci. Int.*, vol. 302, p. 109838, 2019, doi: 10.1016/j.forsciint.2019.05.054.
[40] B. G. Ioan, C. Manea, B. Hanganu, L. Statescu, L. G. Solovastru, and I. Manoilescu, "The chemistry decomposition in human corpses," *Rev. Chim.*, vol. 68, no. 6, pp. 1450–1454, 2017, doi: 10.37358/rc.17.6.5672.
[41] L. Iancu, E. N. Junkins, G. Necula-Petrareanu, and C. Purcarea, "Characterizing forensically important insect and microbial community colonization patterns in buried remains," *Sci. Rep.*, vol. 8, no. 1, pp. 1–16, 2018, doi: 10.1038/s41598-018-33794-0.
[42] J. M. DeBruyn and K. A. Hauther, "Postmortem succession of gut microbial communities in deceased human subjects," *PeerJ*, vol. 2017, no. 6, pp. 1–14, 2017, doi: 10.7717/peerj.3437.

APPENDIX – Figures & Tables

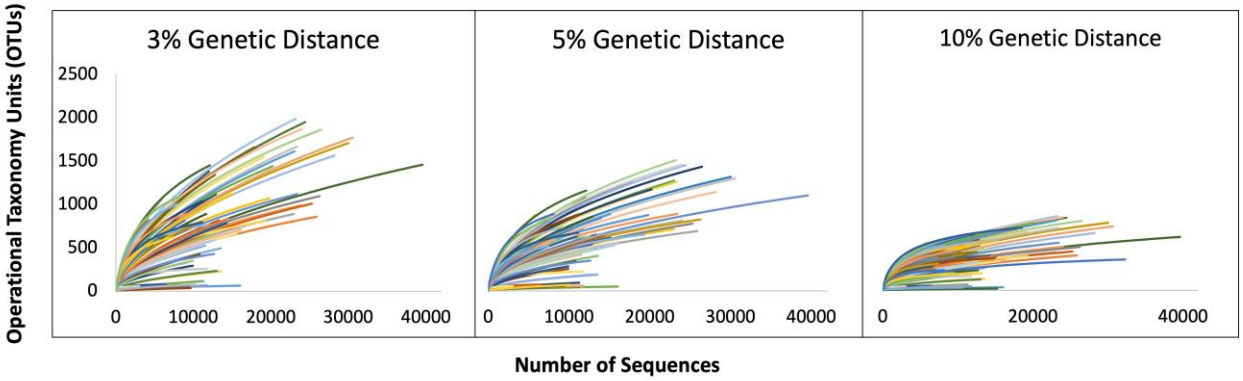

Figure 1: Rarefaction curve showing number of OTUs over sequencing cycles at 3%, genetic distance.

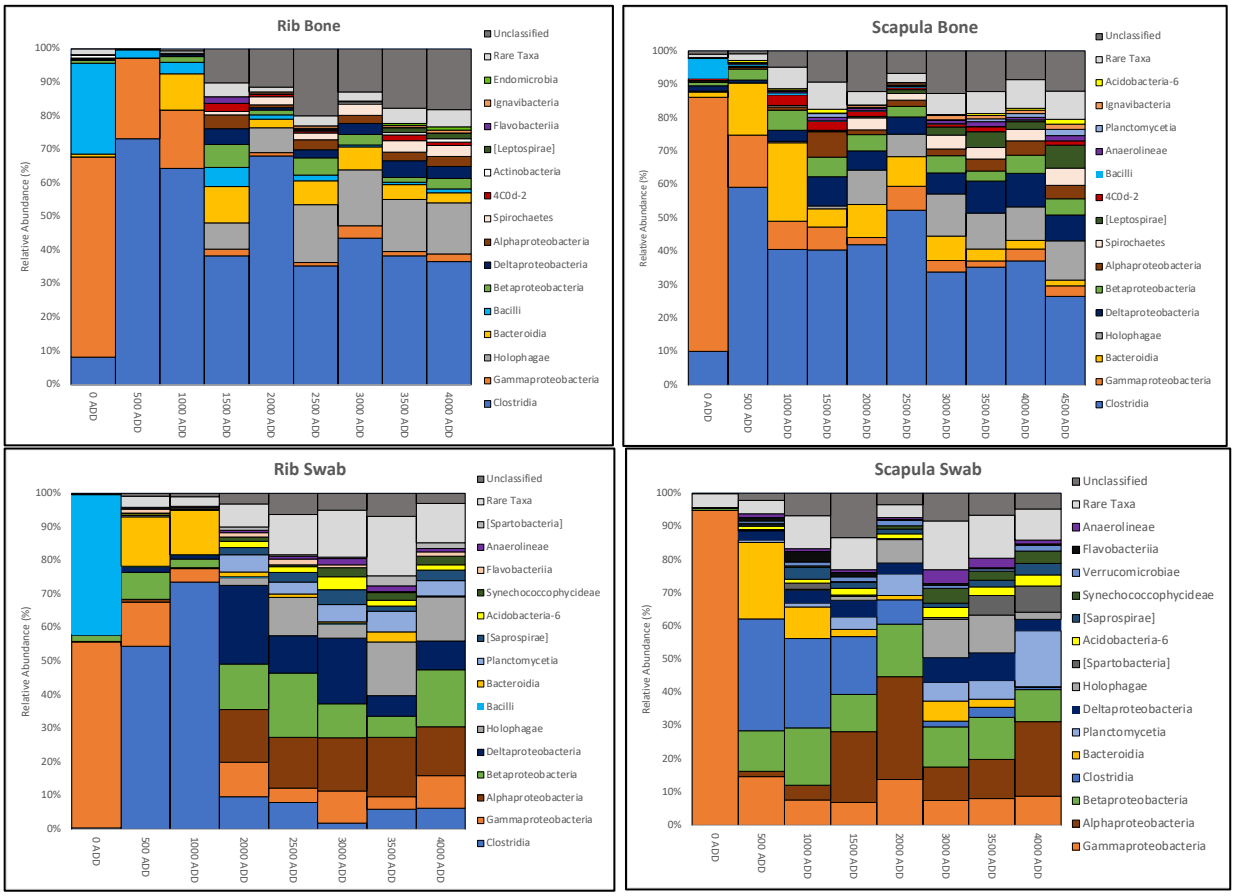

Figure 2: Relative abundance across accumulated degree days (ADD) at the class level for bone and swab samples.

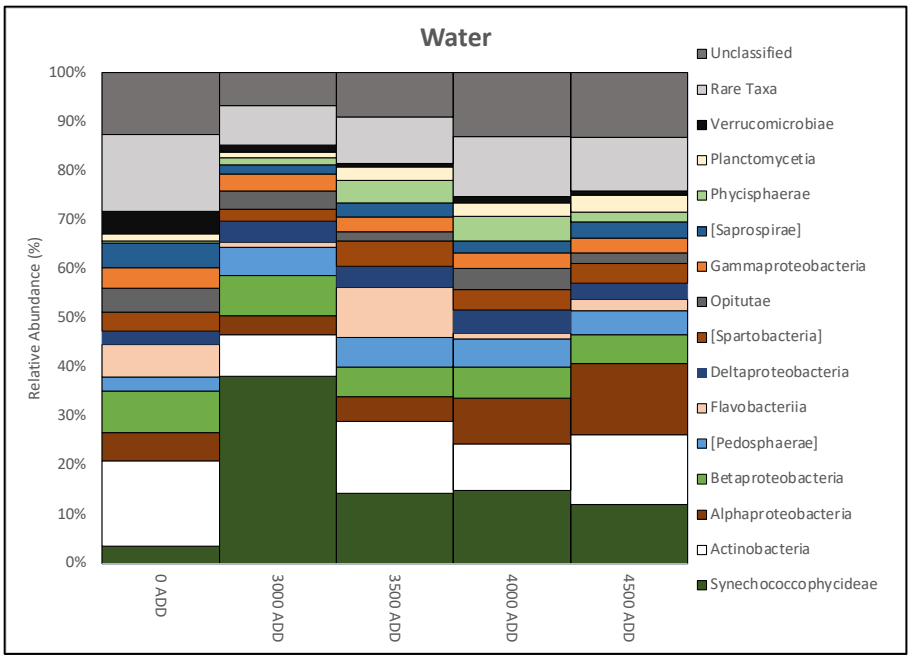

Figure 3: Relative abundance for water across accumulated degree days (ADD) at the class level.

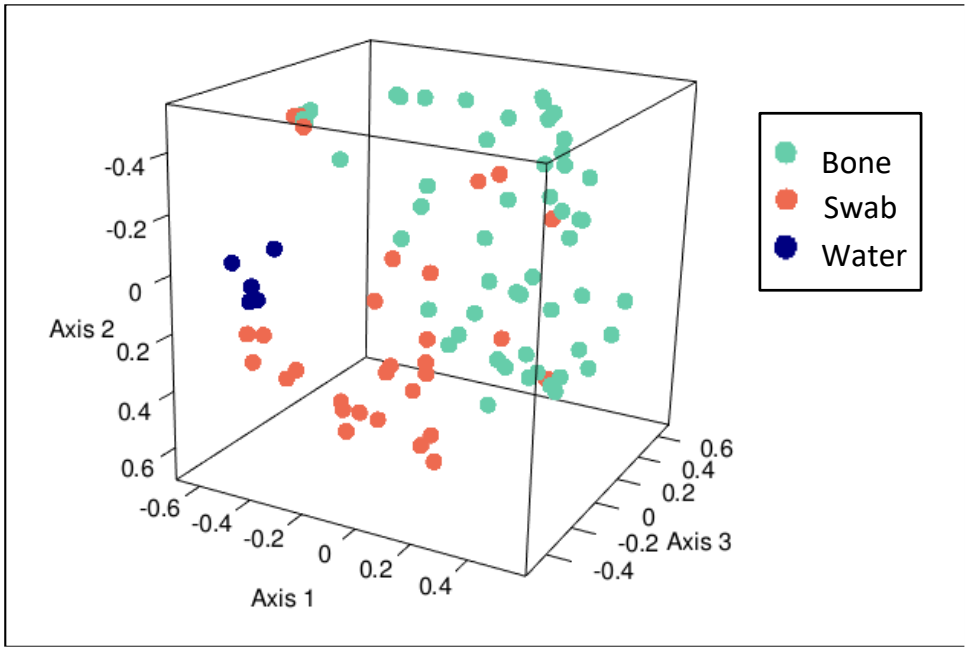

Figure 4: Three-dimensional nonmetric dimensional scaling (NMDS) ordination plot of the Yue & Clayton distance 5% genetic distance for bone, swab, and water samples (R^2 = 0.682347; lowest stress = 0.215).

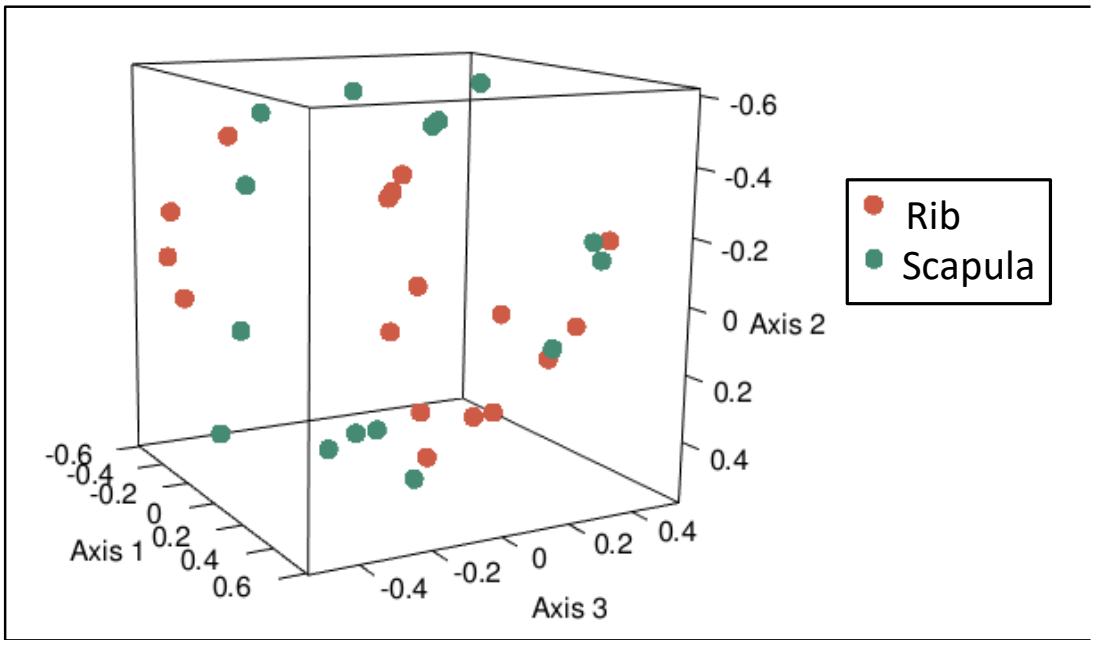

Figure 5: Three-dimensional nonmetric dimensional scaling (NMDS) ordination plot of the Yue & Clayton distance based on 5% genetic distance for rib and scapula swab samples (R^2 = 0.726; lowest stress = 0.191).

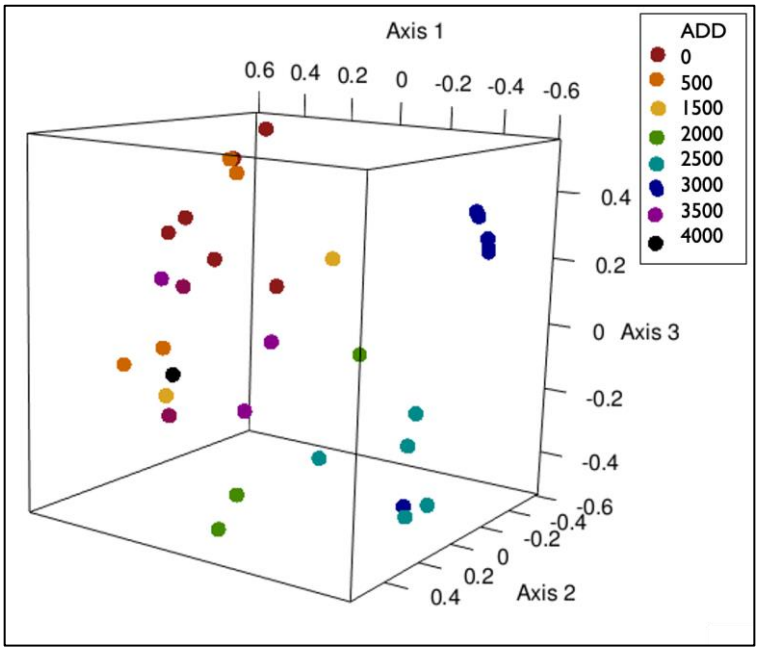

Figure 6: Three-dimensional nonmetric dimensional scaling (NMDS)ordination plot of the Yue & Clayton distance 5% genetic distance for swab samples across ADD (R^2 = 0.726; lowest stress = 0.191).

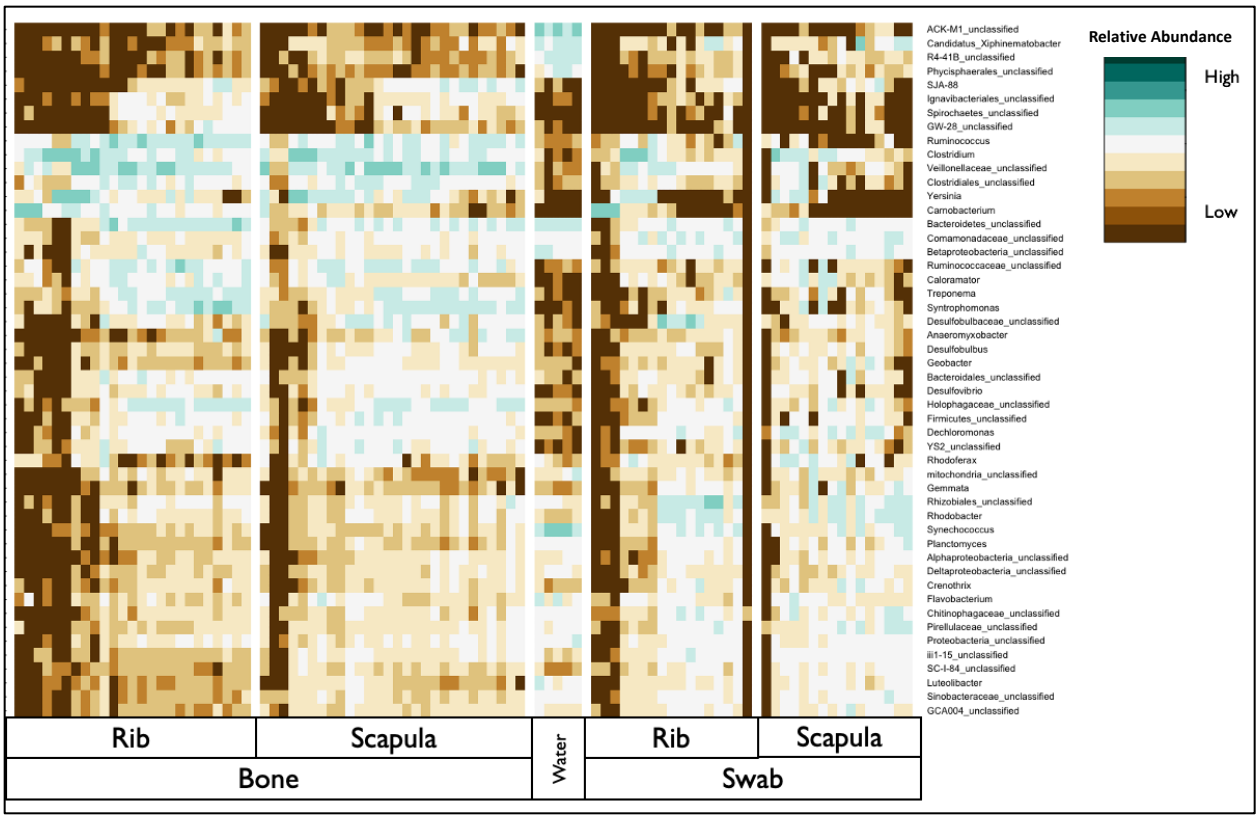

Figure 7: Heat map of indicator genera for bone, water, and swab samples, with lower relative abundance denoted in brown, and higher relative abundance in teal.

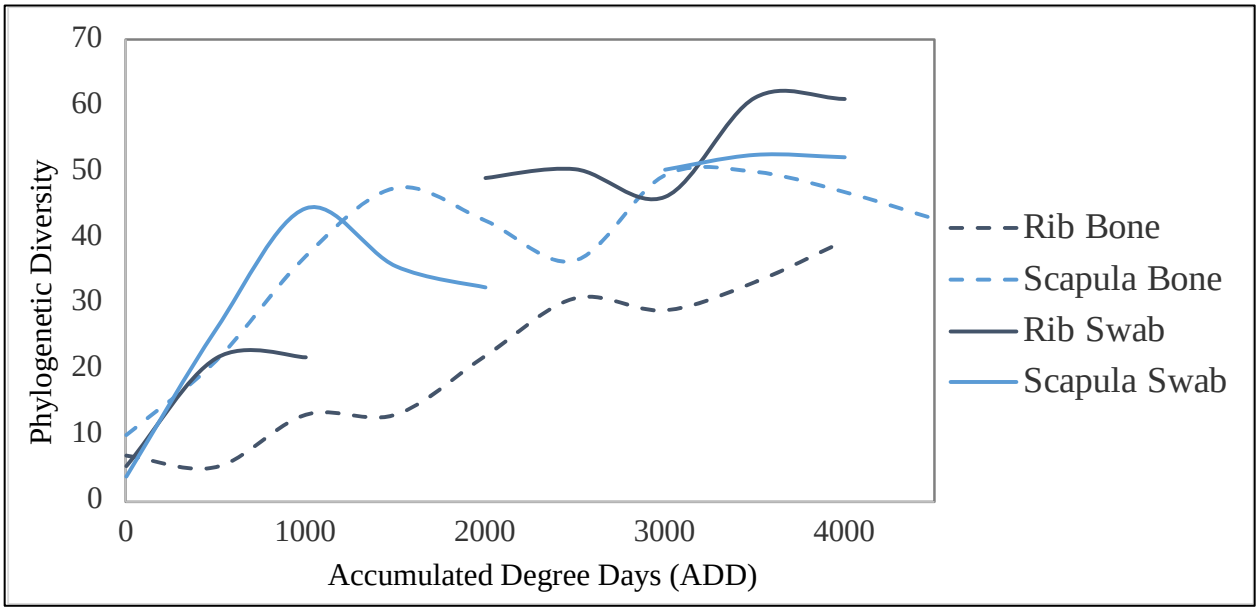

Figure 8: Phylogenetic alpha diversity for bone and swab samples across accumulated degree days (ADD).

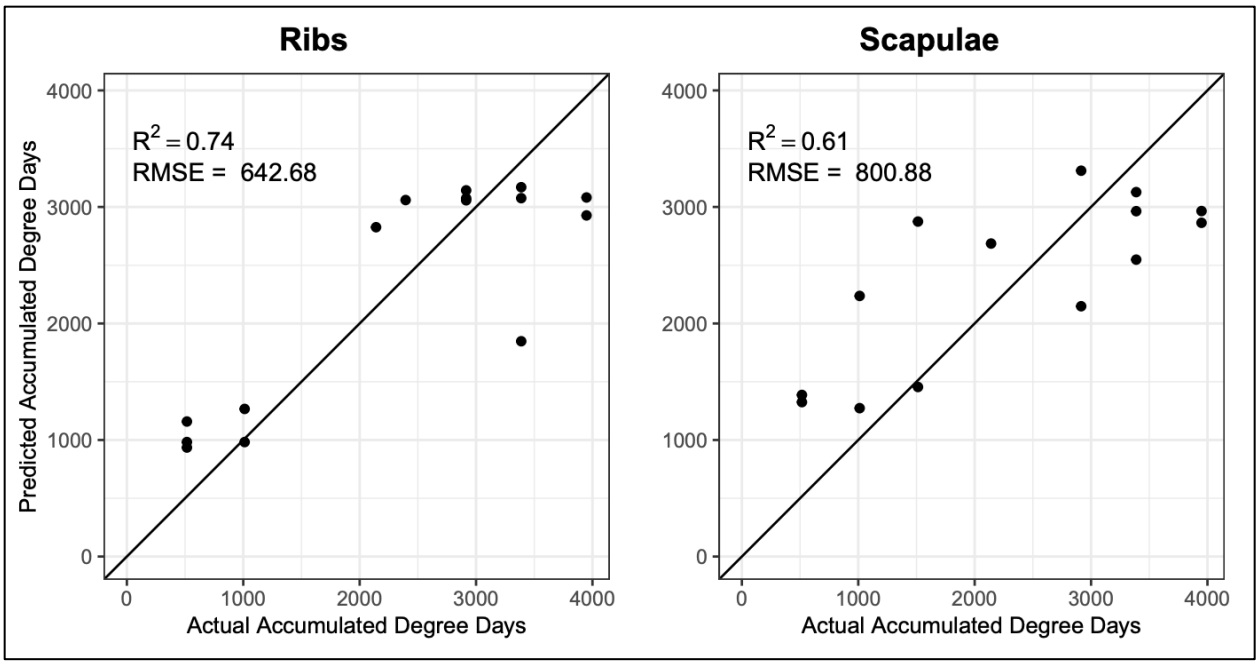

Figure 9: Rib and scapula swab PMSI models produced using Random Forest Modeling, excluding baseline (0 ADD) observations.

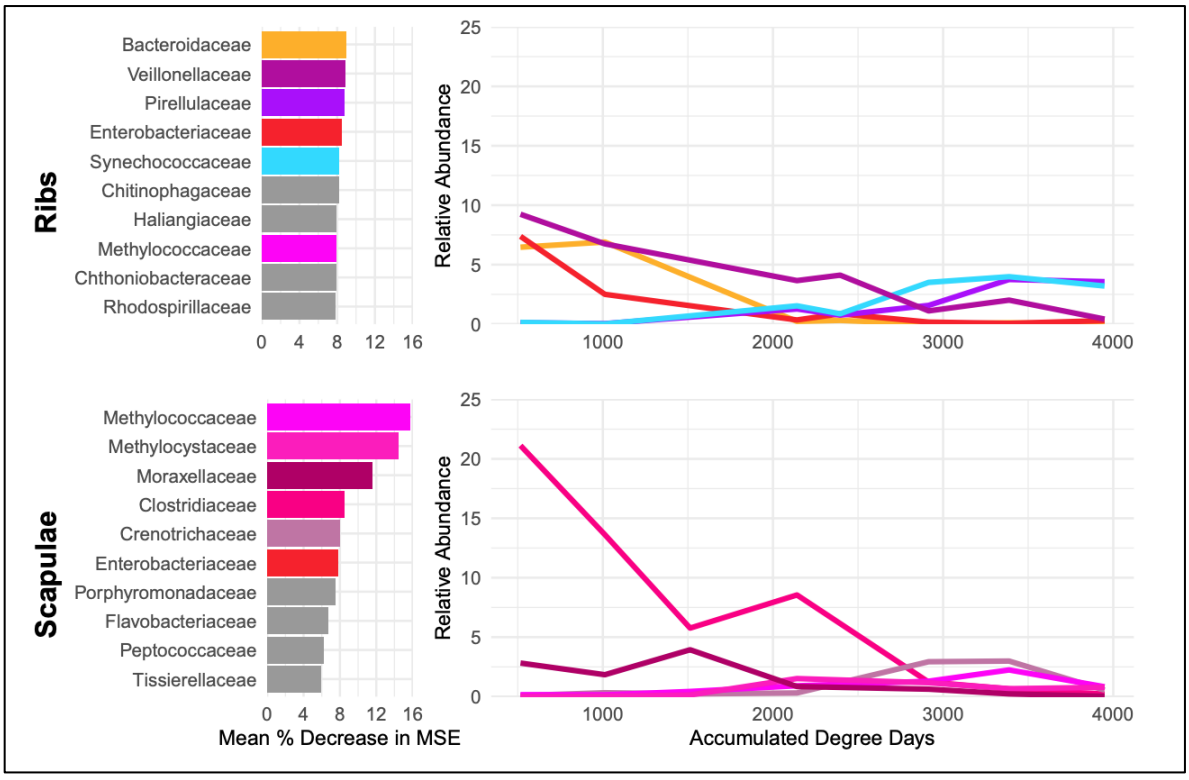

Figure 10: Influential taxa used to inform the random forest model (top five influential taxa in color. Note: Methylococcaceae pictured in color in the rib taxa to note this taxon appeared in the scapula influential taxa.

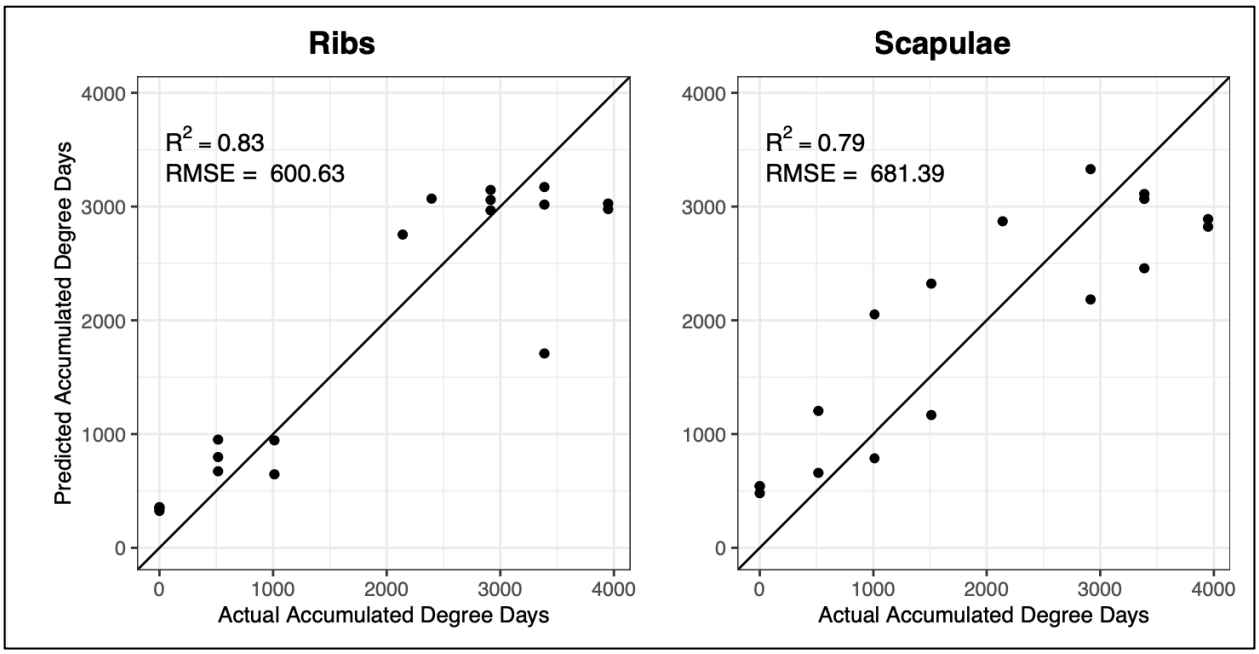

Figure 11: Rib and scapula swab PMSI models produced using random forest modeling, including baseline (0 ADD) observations.

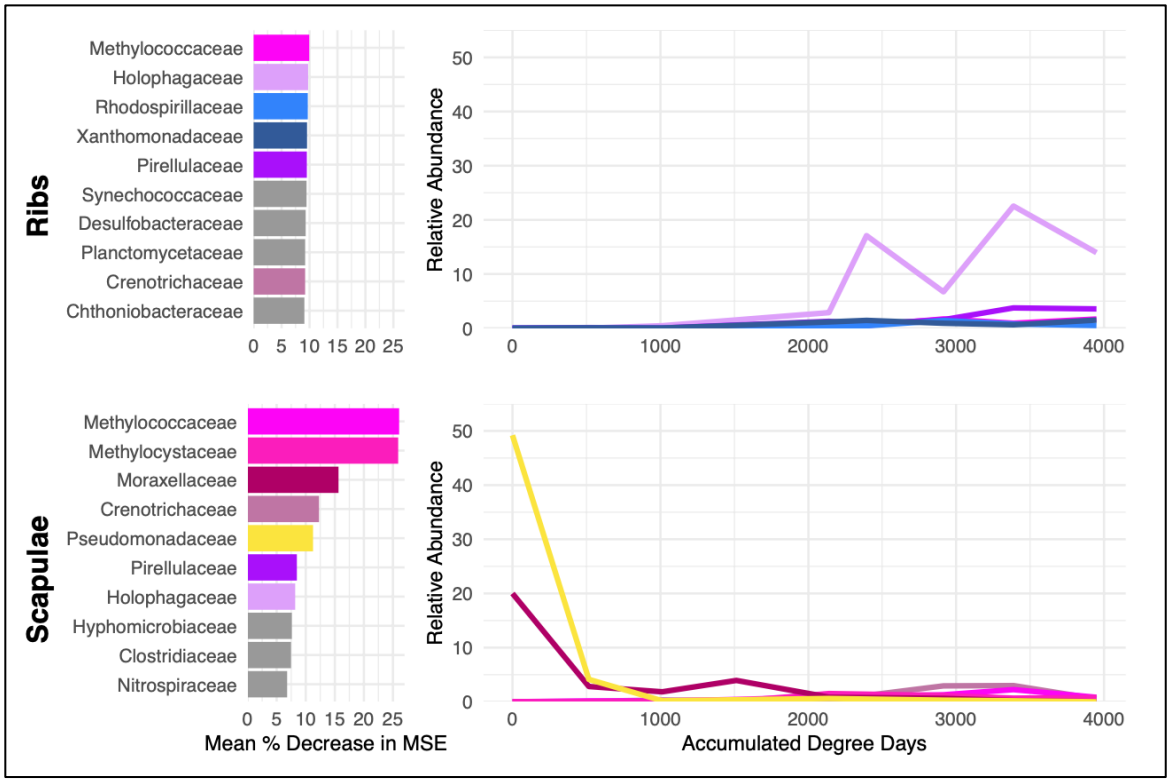

Figure 12: Influential taxa used to inform the random forest model (top five influential taxa in color. Note: Crenotrichaceae and Holophagaceae pictured in color in the rib and scapula taxa, respectively, to note that these taxa also appeared in the scapula and rib influential taxa.

Table 1: Samples used for analysis with time since deposition, collection identifier (ID), and the corresponding expected and actual accumulated degree days (ADD). Note: Ribs 2 and 3 from collection 6 were lost during submersion.

Expected ADD	Actual ADD	Time Since Deposition (Days)	Collection ID	Rib Swab Samples	Rib Bone Samples	Scapulae Swab Samples	Scapulae Bone Samples
0	0	0	Baseline	SARRRR1B SARRRR2B SARRRR3B	RRR1BCS RRR2BCS RRR3BCS	SARRRS1B SARRRS2B SARRRS3B	RRS1BCS RRS2BCS RRS3BCS
500	516	81	Collection 2	SARRRR1C2 SARRRR2C2 SARRRR3C2	RRR1C2CS RRR2C2CS RRR3C2CS	SARRRS1C2 SARRRS2C2 SARRRS3C2	RRS1C2CS RRS2C2CS RRS3C2CS
1000	1012	132	Collection 4	SARRRR1C4 SARRRR2C4 SARRRR3C4	RRR1C4CS RRR2C4CS RRR3C4CS	SARRRS1C4 SARRRS2C4 SARRRS3C4	RRS1C4CS RRS2C4CS RRS3C4CS
1500	1513	166	Collection 6	SARRRR1C6	RRR1C6CS	SARRRS1C6 SARRRS2C6 SARRRS3C6	RRS1C6CS RRS2C6CS RRS3C6CS
2000	2141	193	Collection 8	SARRRR1C8 SARRRR2C8 SARRRR3C8	RRR1C8CS RRR2C8CS RRR3C8CS	SARRRS1C8 SARRRS2C8 SARRRS3C8	RRS1C8CS RRS2C8CS RRS3C8CS
2500	2395	203	Collection 9	SARRRR1C9 SARRRR2C9 SARRRR3C9	RRR1C9CS RRR2C9CS RRR3C9CS	SARRRS1C9 SARRRS2C9 SARRRS3C9	RRS1C9CS RRS2C9CS RRS3C9CS
3000	2915	222	Collection 11	SARRRR1C11 SARRRR2C11 SARRRR3C11	RRR1C11CS RRR1C11CS RRR3C11CS	SARRRS1C11 SARRRS2C11 SARRRS3C11	RRS1C11CS RRS1C11CS RRS3C11CS
3500	3388	238	Collection 13	SARRRR1C13 SARRRR2C13 SARRRR3C13	RRR1C13CS RRR1C13CS RRR3C13CS	SARRRS1C13 SARRRS2C13 SARRRS3C13	RRS1C13CS RRS1C13CS RRS3C13CS
4000	3949	258	Collection 15	SARRRR1C15 SARRRR2C15 SARRRR3C15	RRR1C15CS RRR1C15CS RRR3C15CS	SARRRS1C15 SARRRS2C15 SARRRS3C15	RRS1C15CS RRS1C15CS RRS3C15CS
4500	4473	276	Collection 17	SARRRR1C17 SARRRR2C17 SARRRR3C17	RRR1C17CS RRR1C17CS RRR3C17CS	SARRRS1C17 SARRRS2C17 SARRRS3C17	RRS1C17CS RRS1C17CS RRS3C17CS

Table 2: Initial number of sequence reads for rib and scapula samples for bones and swabs.

Bone Samples				Swab Samples				Water	
Rib Sample ID	Reads	Scapula Sample ID	Reads	Rib Sample ID	Reads	Scapula Sample ID	Reads	Sample ID	Reads
RRR1BCS	9480	RRS1BCS	15189	SARRRR1B	10491	SARRRS1B	21149	RRWBCS	14481
RRR2BCS	7499	RRS2BCS	13904	SARRRR2B	15075	SARRRS2B	18646	RRWC2CS	54
RRR3BCS	9074	RRS3BCS	10574	SARRRR3B	16039	SARRRS3B	14968	RRWC4CS	69
RRR1C2CS	13111	RRS1C2CS	13738	SARRRR1C2	20588	SARRRS2C2	18639	RRWC6CS	40
RRR2C2CS	13060	RRS2C2CS	12374	SARRRR2C2	15616	SARRRS3C2	11975	RRWC8CS	64
RRR3C2CS	14742	RRS3C2CS	20907	SARRRR3C2	11012	SARRRS1C4	19935	RRWC9CS	200
RRR1C4CS	13447	RRS1C4CS	16345	SARRRR1C4	759	SARRRS3C4	13621	RRWC11CS	33923
RRR3C4CS	17284	RRS2C4CS	19377	SARRRR2C4	58662	SARRRS1C6	9138	RRWC13CS	46835
RRR1C6CS	17683	RRS3C4CS	16121	SARRRR1C8	13839	SARRRS3C6	12400	RRWC15CS	43133
RRR2C4CS	17631	RRS1C6CS	16749	SARRRR2C9	14004	SARRRS3C8	13586	RRWC17CS	33586
RRR1C8CS	13190	RRS2C6CS	22928	SARRRR1C11	7590	SARRRS2C11	13294		
RRR2C8CS	17912	RRS3C6CS	18883	SARRRR2C11	11257	SARRRS3C11	12852		
RRR3C8CS	16155	RRS1C8CS	18791	SARRRR3C11	18383	SARRRS1C13	20437		
RRR1C9CS	20606	RRS2C8CS	15747	SARRRR1C13	15818	SARRRS2C13	13979		
RRR2C9CS	17983	RRS3C8CS	14101	SARRRR2C13	11423	SARRRS3C13	30329		
RRR3C9CS	21273	RRS1C9CS	16987	SARRRR3C13	21369	SARRRS1C15	18882		
RRR1C11CS	46315	RRS2C9CS	15818	SARRRR1C15	17961	SARRRS2C15	18846		
RRR3C11CS	42846	RRS3C9CS	19433	SARRRR2C15	10890				
RRR1C13CS	45035	RRS1C11CS	41511						
RRR2C13CS	47033	RRS2C11CS	66096						
RRR3C13CS	57148	RRS3C11CS	57355						
RRR1C15CS	36099	RRS1C13CS	51904						
RRR2C15CS	39094	RRS2C13CS	51930						
RRR3C15CS	56073	RRS3C13CS	56618						
		RRS1C15CS	49714						
Negative Controls		RRS2C15CS	31392	Negative Controls		Positve Control			
Negative257	3740	RRS3C15CS	41197	SARNEG	3	SARMOCK	13930		
Negative258	37387	RRS1C17CS	10734						
Negative303	18219	RRS2C17CS	26455						
Negative306	10790	RRS3C17CS	7225						

Table 3: Final number of sequence reads for rib and scapula samples for bones and swabs.

Bone Samples				Swab Samples				Water	
Rib Sample ID	Reads	Scapula Sample ID	Reads	Rib Sample ID	Reads	Scapula Sample ID	Reads	Sample ID	Reads
RRR1BCS	7947	RRS1BCS	11767	SARRRR1B	7516	SARRRS1B	4229	RRWBCS	5868
RRR2BCS	4925	RRS2BCS	11829	SARRRR2B	9377	SARRRS2B	15236	RRWC2CS	15
RRR3BCS	6462	RRS3BCS	9453	SARRRR3B	5398	SARRRS3B	10680	RRWC4CS	12
RRR1C2CS	11298	RRS1C2CS	10826	SARRRR1C2	12698	SARRRS2C2	13195	RRWC6CS	4
RRR2C2CS	11547	RRS2C2CS	9923	SARRRR2C2	8106	SARRRS3C2	7026	RRWC8CS	21
RRR3C2CS	11403	RRS3C2CS	15636	SARRRR3C2	12346	SARRRS1C4	12470	RRWC9CS	23
RRR1C4CS	9944	RRS1C4CS	12032	SARRRR1C4	9503	SARRRS3C4	9568	RRWC11CS	15099
RRR3C4CS	13016	RRS2C4CS	14302	SARRRR2C4	541	SARRRS1C6	6589	RRWC13CS	23047
RRR1C6CS	13349	RRS3C4CS	12728	SARRRR1C8	32291	SARRRS3C6	7342	RRWC15CS	20234
RRR2C4CS	13546	RRS1C6CS	12793	SARRRR2C9	4274	SARRRS3C8	8166	RRWC17CS	11192
RRR1C8CS	9018	RRS2C6CS	17875	SARRRR1C11	10202	SARRRS2C11	7156		
RRR2C8CS	13610	RRS3C6CS	13970	SARRRR2C11	11268	SARRRS3C11	8305		
RRR3C8CS	11547	RRS1C8CS	12906	SARRRR3C11	11155	SARRRS1C13	14829		
RRR1C9CS	15190	RRS2C8CS	10435	SARRRR1C13	7406	SARRRS2C13	9420		
RRR2C9CS	12839	RRS3C8CS	8858	SARRRR2C13	11169	SARRRS3C13	18542		
RRR3C9CS	16199	RRS1C9CS	11673	SARRRR3C13	12147	SARRRS1C15	14064		
RRR1C11CS	25856	RRS2C9CS	10967	SARRRR1C15	7852	SARRRS2C15	15348		
RRR3C11CS	25274	RRS3C9CS	14512	SARRRR2C15	10890				
RRR1C13CS	23008	RRS1C11CS	19152						
RRR2C13CS	23425	RRS2C11CS	30599						
RRR3C13CS	26279	RRS3C11CS	24464						
RRR1C15CS	19853	RRS1C13CS	23230						
RRR2C15CS	24012	RRS2C13CS	23380						
RRR3C15CS	30050	RRS3C13CS	28246						
		RRS1C15CS	26501						
Negative Controls		RRS2C15CS	19357	Negative Controls		Positve Control			
Negative257	657	RRS3C15CS	23991	SARNEG	1	SARMOCK	9665		
Negative258	257	RRS1C17CS	3420						
Negative303	1231	RRS2C17CS	12555						
Negative306	1155	RRS3C17CS	3050						

Table 4: Analysis of Molecular Variance (AMOVA) detected significant differences in sample type (p-value: <0.001, F = 6.32137) of sample type (bone, swab, and water) with p-values and F statistics for pairwise comparisons

	Swab	Water
Bone	p<0.001 F=6.7147	p<0.001 F=6.9662
Swab		p<0.001 F=4.54139

Table 5: Analysis of Molecular Variance (AMOVA) test of sample type and bone type (p<0.001, F=4.29435) with p-values and F statistics for pairwise comparisons.

	Scapula Bone	Rib Swab	Scapula Swab	Water
Rib Bone	0.002 F=2.96807	<0.001 F=3.57805	<0.001 F=5.10984	<0.001 F=6.84472
Scapula Bone		<0.001 F=4.04834	<0.001 F=4.76262	<0.001 F=7.29137
Rib Swab			0.262 F=1.20142	<0.001 F=4.7274
Scapula Swab				<0.001 F=4.13137

Table 6: Summary of Analysis of Molecular Variance (AMOVA) results for accumulated degree days (ADD) for rib and scapula swab samples (p<0.001, F= 3.67184) with summary significance values.

ADD	500	1000	1500	2000	2500	3000	3500	4000
0	**	*	*	*	NS	**	**	**
500		NS	NS	*	NS	**	**	**
1000			NS	NS	NS	*	**	*
1500				NS	NS	NS	*	NS
2000					NS	NS	NS	NS
2500						NS	NS	NS
3000							NS	NS
3500								NS

* = p<0.05
** = p<0.01
*** = p<0.001
NS = not significant (p>0.05)

Table 7: Top 12 indicator genera for all samples. Note: samples shown represent all samples and combinations of samples with PBCC values >0.5.

Genera	Indicator Group	PBCC	P-value
ACK.M1_unclassified	Water	0.96	0.0001
R4.41B_unclassified	Water	0.918	0.0001
Phycisphaerales_unclassified	Water	0.783	0.0001
Synechococcus	Water	0.747	0.0001
Proteobacteria_unclassified	Water	0.656	0.0002
Sinobacteraceae_unclassified	swab_rib+swab_scap+Water	0.621	0.0002
Ruminococcus	bone_rib+bone_scap	0.602	0.0006
Chitinophagaceae_unclassified	swab_rib+swab_scap+Water	0.583	0.0009
Bacteroidetes_unclassified	bone_rib+Water	0.566	0.001
SC.I.84_unclassified	swab_rib+swab_scap	0.566	0.0012
Treponema	bone_rib+bone_scap	0.544	0.0015
Luteolibacter	Water	0.539	0.001

Table 8: Top indicator genera for water, bone powder, and swab samples.

Genera	Indicator Group	PBCC	P-value
ACK.M1_unclassified	Water	0.96	0.0001
R4.41B_unclassified	Water	0.918	0.0001
Phycisphaerales_unclassified	Water	0.783	0.0001
Synechococcus	Water	0.747	0.0001
Proteobacteria_unclassified	Water	0.656	0.0002
Luteolibacter	Water	0.539	0.001
Deltaproteobacteria_unclassified	Water	0.518	0.0035
Flavobacterium	Water	0.454	0.0059
mitochondria_unclassified	Water	0.351	0.0445
GW.28_unclassified	Bone Powder	0.459	0.0091
YS2_unclassified	Bone Powder	0.45	0.0083
SJA.88	Bone Powder	0.388	0.027
Anaeromyxobacter	Bone Powder	0.346	0.0452
Desulfobulbaceae_unclassified	Swab	0.386	0.0219
Dechloromonas	Swab	0.435	0.0098
Rhodoferax	Swab	0.416	0.0155
Pirellulaceae_unclassified	Swab	0.399	0.0155
GCA004_unclassified	Swab	0.399	0.0188

Table 9: Top indicator genera for bone and swab samples.

Genera	Indicator Group	PBCC	P-value
GW.28_unclassified	Rib Bone	0.459	0.0091
YS2_unclassified	Scapula Bone	0.45	0.0083
SJA.88	Scapula Bone	0.388	0.027
Anaeromyxobacter	Scapula Bone	0.346	0.0452
Desulfobulbaceae_unclassified	Rib Swab	0.386	0.0219
Dechloromonas	Scapula Swab	0.435	0.0098
Rhodoferax	Scapula Swab	0.416	0.0155
Pirellulaceae_unclassified	Scapula Swab	0.399	0.0155
GCA004_unclassified	Scapula Swab	0.399	0.0188

Table 10: Inverse Simpson Index, Shannon Index, and Shannon Evenness Index values for alpha diversity for bone, swab, and water samples by bone type.

Rib Samples										
ADD	Actual ADD	Inverse Simpson Index			Shannon Index			Shannon Evenness Index		
		Swab	Bone	Water	Swab	Bone	Water	Swab	Bone	Water
0	0	4.08	3.35	62.74	2.04	1.49	5.17	0.48	0.39	0.77
500	516	13.78	33.98	-	3.65	4.77	-	0.62	0.75	-
1000	1012	19.59	40.14	-	4.03	5.11	-	0.67	0.77	-
1500	1513	24.15	33.78	-	4.22	4.18	-	0.68	0.70	-
2000	2141	3.77	23.97	-	1.54	4.36	-	0.44	0.72	-
2500	2395	7.64	13.28	-	2.50	3.05	-	0.54	0.56	-
3000	2915	8.75	27.27	6.97	3.10	4.70	3.88	0.57	0.74	0.62
3500	3388	23.71	26.58	23.29	3.99	3.71	4.54	0.67	0.64	0.71
4000	3949	8.68	46.31	32.63	2.84	3.91	4.78	0.57	0.66	0.75
4500	4473	23.50	38.98	34.30	4.17	4.68	4.90	0.69	0.75	0.76
Scapula Samples										
ADD	Actual ADD	Inverse Simpson Index			Shannon Index			Shannon Evenness Index		
		Swab	Bone	Water	Swab	Bone	Water	Swab	Bone	Water
0	0	5.26	2.15	62.74	1.86	1.10	5.17	0.41	0.35	0.77
500	516	32.75	42.61	-	4.63	5.09	-	0.72	0.78	-
1000	1012	25.21	40.43	-	4.47	5.01	-	0.70	0.75	-
1500	1513	16.98	27.18	-	4.19	4.56	-	0.66	0.73	-
2000	2141	27.86	34.59	-	3.91	4.22	-	0.67	0.72	-
2500	2395	24.53	12.58	-	3.77	2.79	-	0.64	0.53	-
3000	2915	19.46	28.16	6.97	4.02	4.74	3.88	0.65	0.75	0.62
3500	3388	25.02	32.82	23.29	4.22	2.78	4.54	0.66	0.41	0.71
4000	3949	16.94	10.61	32.63	3.80	2.11	4.78	0.62	0.36	0.75
4500	4473	31.44	-	34.30	3.51	-	4.90	0.59	-	0.76

- indicates no value due to insufficient data for analysis.

VITA

Sarah Rose is from New York City and the Hudson Valley Region of New York. She graduated from East Stroudsburg University of Pennsylvania with a Bachelor's degree in Biology and Environmental Studies with a minor in Chemistry. She's been involved in various marine research and conservation projects, including working for the National Park Service, the Georgia Department of Natural Resources, and the Virginia Aquarium before pursuing coursework in forensic science. Sarah is currently a second-year master's student at Virginia Commonwealth University in the Forensic Science Department. She is also the Lab Manager for the Simmons Forensic Anthropology Research Laboratory and Research Coordinator for VCU's East Marshall Street Well Project.